Synthesis of monodisperse Fe@SiO_2 core-shell nanocapsules and investigation of their magnetic behaviour

Wen Zeng, Qiqi Yang, Bin Shao ✉, Donglin Guo, Chunhong Li, Yilong Ma, Xueguo Yin, Sibo Zhao, Kejian Li

School of Metallurgy and Materials Engineering, Chongqing University of Science and Technology, 401331 Chongqing, People's Republic of China
✉ *E-mail: shaobin19811107@163.com*

Published in Micro & Nano Letters; Received on 24th January 2019; Revised on 22nd March 2019; Accepted on 17th April 2019

The monodisperse Fe@SiO_2 core-shell nanocapsules were synthesised via hydrothermal reaction followed with heat treatment. Nanostructures were characterised by X-ray diffraction, scanning electron microscopy and transmission electron microscopy. The magnetic properties of Fe@SiO_2 nanocapsules were evaluated with magnetic property measurement system. The results show that Fe@SiO_2 core-shell nanocapsules are highly monodispersed. The silica thickness of Fe@SiO_2 nanocapsules increased from 10–20 to 25–35 nm with increasing tetraethyl orthosilicate (TEOS) amount. In the Fe@SiO_2 nanocapsules prepared with 900 µl TEOS, as the reaction temperature increases, the mean particle size of Fe@SiO_2 nanocapsules increases from 328 to 546 nm. It is remarkable that the saturation magnetisation of Fe@SiO_2 nanocapsules decreases with increasing silica thickness. However, the coercivity of nanocapsules has less influence with the variation of silica thickness and particles' length.

1. Introduction: Nanomaterials are subjected to extensive research efforts due to their exceptional surface effects, quantum size effects and macroscopical quantum tunnel effects compared with conventional materials [1, 2]. Nanomaterials can be classified into three types, namely discrete nanomaterials, nanoscale device materials and bulk nanomaterials [3]. Discrete nanomaterials are material elements that are freestanding and in the range of 1–10 nm in scale as zero-dimensional (0D) (particles) or 1D (fibres) [3]. Nanoscale device materials are nanoscale material elements that are contained within devices, usually as 2D (thin films) [3]. Bulk nanomaterials are materials that are available in bulk quantities and usually as 3D [3]. However, some potential applications and properties of nanoparticles are limited due to their propensity to be easily agglomeration and oxidisation. In order to address these problems, several methods have been investigated. The most widely reported method is to coat the nanoparticles with a protective shell to form core-shell nanocomposites. The materials of protective shell include silica [4–10], carbon [11, 12], titanium oxide [13, 14], polymers [15] etc. The core-shell nanocomposites have many potential applications, such as drug delivery, bioimaging, catalytic, electronic, microwave absorbents and environmental remediation [16–21].

Iron (Fe) nanocomposites have been attracting great attention because of their low cost and wide applications. Fe nanocomposites have good magnetic properties. The Fe@SiO_2/polymer nanocomposites have higher magnetodielectric properties [dielectric permittivity (ε), dielectric loss (tan δ), magnetic permeability (μ)] at radio frequencies (1 MHz–1 GHz), renders it as a good candidate for dielectric applications [7]. The Fe@SiO_2 nanoparticles exhibit superferromagnetism properties, renders it as a good candidate for microelectronics applications [5, 8]. In addition, nanoscale zero-valent iron (NZVI) nanocomposites are well-known for their application in environmental fields due to their small particle size, large surface area and high in situ reactivity. NZVI nanocomposites are widely used to remove Cr^{6+} [19, 22–24], nitrate [25–27] and other metal ions (Co^{2+}, Cu^{2+}, Fe^{2+}, Be^{2+}, Zn^{2+}, Hg^{2+} etc.) [20, 28, 29]. Obviously, particle size and degree of dispersion are important factors that affect the use of Fe nanocomposites. Although there have been many studies on the preparation of iron nanocomposites, however, the studies on the preparation of monodisperse Fe nanorods are still rare.

In this research, highly monodisperse Fe@SiO_2 core-shell nanocapsules were synthesised by hydrothermal reaction followed with heat treatment. Nanostructures were characterised by X-ray diffraction (XRD), scanning electron microscopy (SEM) and transmission electron microscopy (TEM). The magnetic properties of the Fe@SiO_2 core-shell nanocapsules were investigated at 300 K.

2. Experimental

2.1. Materials and reagents: All chemicals, namely iron chloride hexahydrate ($FeCl_3 \cdot 6H_2O$, 99% AR), tetraethyl orthosilicate (TEOS, 99% GC), polyvinylpyrrolidone (PVP, molecular weight 58,000), ammonia solution (25–28% GR), absolute ethanol (99.7% AR) were purchased from Shanghai Aladdin Bio-Chem Technology Co., LTD and used as received without further purification. Deionised water was prepared in the laboratory and used for the preparation of all the reagents in all of the experiments.

2.2. Synthesis of β-FeOOH nanorods: The β-FeOOH nanorods were synthesised by hydrothermal reaction. $FeCl_3 \cdot 6H_2O$ was dissolved in deionised water and the concentration of Fe^{3+} adjusted to 0.02 M. Studies have shown that the morphology and size of β-FeOOH can be adjusted by varying the concentrations of $FeCl_3$, reaction temperature, electrolytes and surfactants [30]. In order to obtain β-FeOOH nanorods with different sizes, the solution was heated at 90 and 120°C, respectively. For β-FeOOH nanorods synthesised at 90°C, the solution was poured into a round-bottomed flask and stirred mechanically for 8 h to obtain uniformly distributed β-FeOOH nanorods. For β-FeOOH nanorods synthesised at 120°C, the solution was transferred into a stainless steel autoclave with a Teflon liner of 50 ml capacity. The β-FeOOH nanorods were isolated and separated by centrifugation, washed with water and ethanol, and finally dried in an oven at 60°C.

2.3. Synthesis of β-FeOOH@SiO_2 nanocapsules: The synthesis of silica-coated β-FeOOH was carried out using a modified version of the Stöber method. 0.2 g of β-FeOOH nanorods and 1.2 g of PVP were dissolved in 100 ml deionised water. The solution was put under sonication for 15 min and mechanically stirred for 12 h. Subsequently, the solution was isolated by centrifugation. Then, 150 ml ethanol, 15 ml deionised water and 9 ml ammonia solution

doi: 10.1049/mnl.2019.0063

were added. In order to obtain silica shells with different thicknesses, 100 and 900 µl TEOS were added to the solution, respectively. Subsequently, the solution was mechanically stirred for 8 h to mix evenly. The synthesised β-FeOOH@SiO_2 nanocapsules were isolated by centrifugation and washed with deionised water and ethanol, and finally dried in an oven at 60°C.

2.4. Synthesis of Fe@SiO_2 nanocapsules: The synthesised β-FeOOH@SiO_2 nanocapsules were packed in crucible for air heat treatment. The temperature was raised to 500°C in 5°C/min and holding for 4 h, and then decreased to room temperature in 5°C/min. In this way, the α-Fe_2O_3@SiO_2 nanocapsules were obtained. To obtain Fe@SiO_2 nanocapsules, the α-Fe_2O_3@SiO_2 nanocapsules were further heated at 500°C for 10 h under a flow of 300 s.c.c.m. H_2/Ar mixed gas (10% H_2 + 90% Ar, volume ratio).

2.5. Characterisation: The phase compositions of different nanoparticles were studied by X-ray diffraction (smart-Lab) by Cu K_α radiation (45 kV, 200 mA; 2θ range from 10° to 90° with 0.03°/min). The morphology and size of the nanoparticles were characterised by field emission SEM (FE-SEM) (JSM-7800F, JEOL) and high-resolution TEM (HRTEM) (JEM-2100F, JEOL). The magnetic properties of the nanoparticles were obtained using a magnetic property measurement system (MPMS) (MPMS3, Quantum, USA).

3. Results and discussion: Fig. 1 shows the XRD patterns of all the synthesised nanoparticles. From Fig. 1*a*, it can be seen that the pure β-FeOOH (PDF No. 75–1594) nanoparticles were synthesised by hydrolysis of Fe^{3+}. After β-FeOOH@SiO_2 nanoparticles were heating at 500°C for 4 h in air, the α-Fe_2O_3@SiO_2 (PDF No. 79–1741) nanoparticles were obtained, as shown in Fig. 1*b*. Finally, the pure Fe@SiO_2 (PDF No. 65–4899) nanoparticles were obtained by α-Fe_2O_3@SiO_2 nanoparticles calcined H_2/Ar mixed gas and no other phases were identified.

The TEM, HRTEM and SEM images of synthesised nanoparticles prepared at 120°C are presented in Fig. 2. From Fig. 2*a*, it is clear that the β-FeOOH nanoparticles are rod-like and agglomerated seriously. The growth mechanism of rod-like β-FeOOH is as follows [31]. The dissolved Fe^{3+} ions form a complex with water molecules and further form β-FeOOH seeds by hydrolysis reaction. The anions (Cl^-) in solution will interact with the β-FeOOH seeds and incorporate into the tunnel structure. The (100) and (110) surfaces of β-FeOOH have less interaction with the anions (Cl^-) compared with the (001) surface. Finally, β-FeOOH seeds grow along the [001] direction to form a nanorod.

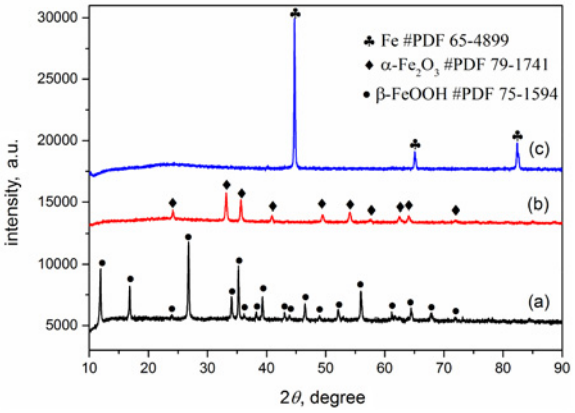

Fig. 1 *X-ray diffraction patterns of the nanoparticles*
a β-FeOOH nanoparticles
b α-Fe_2O_3@SiO_2 nanoparticles
c Fe@SiO_2 nanoparticles

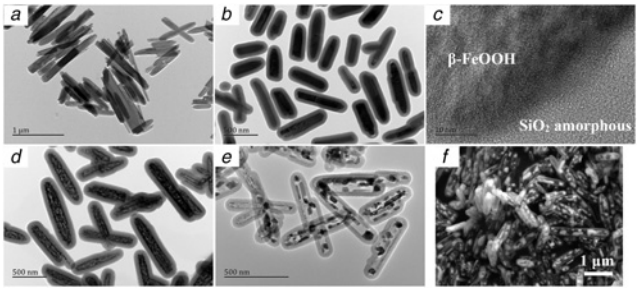

Fig. 2 *TEM, HRTEM and SEM images of nanoparticles prepared at 120°C*
a TEM image of β-FeOOH nanoparticles
b TEM image of silica-coated β-FeOOH nanoparticles
c HRTEM image of silica-coated β-FeOOH nanoparticle
d TEM image of silica-coated α-Fe_2O_3 nanoparticles
e TEM image of silica-coated Fe nanoparticles
f SEM image of silica-coated Fe nanoparticles

After the dispersed and coated silica, monodisperse β-FeOOH@SiO_2 nanorods were obtained, as shown in Fig. 2*b*. Fig. 2*c* shows the HRTEM image of a silica-coated β-FeOOH nanoparticle, it can be seen that the β-FeOOH particle mainly grows along (130) crystal plane with $d_{(130)} = 0.33$ nm. In addition, the coated silica layer is amorphous, which helps improve oxidation-resistance and avoid agglomeration [4, 9, 19]. As Fig. 1 identified, α-Fe_2O_3@SiO_2 nanoparticles were obtained after further calcined in air. As Fig. 2*d* shows, the α-Fe_2O_3 nanoparticles are fluffy and distributed uniformly in the silica shell. To synthesise Fe nanoparticles, α-Fe_2O_3@SiO_2 nanoparticles were further heated under H_2 flow. As depicted in Figs. 2*e* and *f*, the Fe nanoparticles are granular and formed a hollow nanostructure of Fe@SiO_2 core-shell nanocapsules, which is due to the volume reduction from the transformation of α-Fe_2O_3 with a low density of 5.3 g cm^{-3} to denser Fe with a density of 7.86 g cm^{-3}.

Fig. 3 illustrates the morphology and particles length of Fe@SiO_2 nanocapsules prepared at 90 and 120°C. It is clear that the size of Fe@SiO_2 nanocapsules prepared at 120°C is longer than Fe@SiO_2 nanocapsules prepared at 90°C. Figs. 3*c* and *f* represent the distribution map of particles length obtained by analysis of multiple SEM micrographs. It is obvious that the particles length of Fe@SiO_2 nanoparticles prepared at 90°C is in the of range 240–440 nm, and mostly concentrated in 320–360 nm. By counting Fe@SiO_2 nanoparticles from the SEM micrographs the mean particle size was calculated to be 328 nm. By contrast, the particles length of Fe@SiO_2 nanoparticles prepared at 120°C is in the range of 300–900 nm, and mostly concentrated in 400–500 nm. The mean particle size was calculated to be 546 nm. This is mainly due to the effect of reaction temperature, which contributes to the growth of

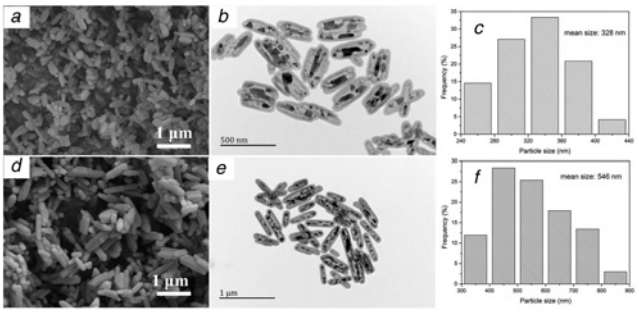

Fig. 3 *SEM, TEM images and histograms showing the particles length of Fe@SiO_2 nanocapsules prepared by hydrothermal reaction at 90°C and 120°C*
a-c 90°C
d-f 120°C

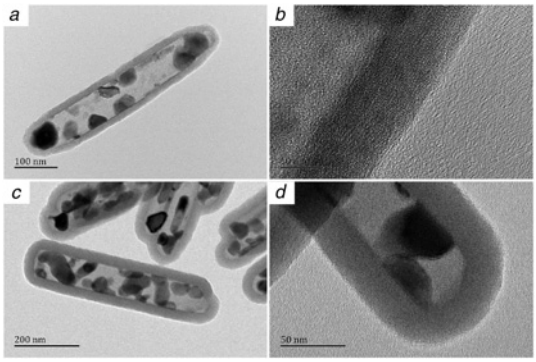

Fig. 4 *TEM images showing the silica thickness of Fe@SiO_2 core-shell nanocapsules prepared at 120°C*
a-b 100 µl TEOS
c-d 900 µl TEOS

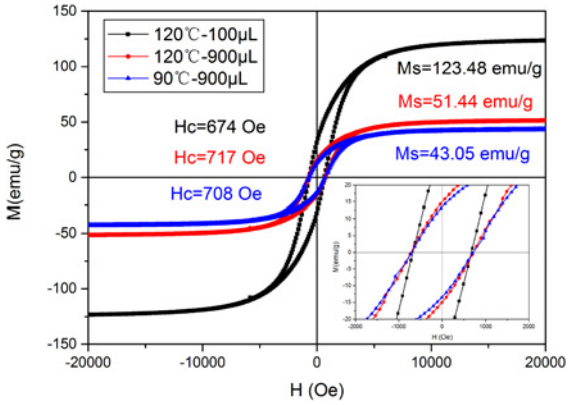

Fig. 5 *Magnetic hysteresis loops of Fe@SiO_2 nanocapsules*

Table 1 Analysis results of particles size of iron in each Fe@SiO_2 nanocapsules. (Fourteen particles were selected from each Fe@SiO_2 nanocapsules for statistics.)

Reaction temperature, °C	TEOS amount, µl	Particles size, nm
90	900	62 ± 15
120	100	63 ± 15
120	900	57 ± 11

particles [30, 32]. Fig. 4 presents the morphology of Fe@SiO_2 nanocapsules prepared at 120°C with different TEOS amount. It is clear that the shell surface of nanocapsules appeared to be quite smooth. The TEM images of the hollow iron nanocapsules show that they are uniform with a shell thickness of 10–20 and 25–35 nm for TEOS with 100 and 900 µl respectively.

The particles size of iron in each Fe@SiO_2 nanocapsules were analysed from the TEM micrographs and the results are listed in Table 1. The results show that the particles size of each nanocapsule is about 60 nm and there is little difference for each nanocapsule. It indicates that the reaction temperature and silica thickness have little effect on the particles size of iron in each nanocapsule.

For comparison the magnetic properties of Fe@SiO_2 nanocapsules with different particle size and shell thickness, the magnetic hysteresis loops of each Fe@SiO_2 nanocapsules in Fig. 5 were measured at 300 K between −20 and 20 kOe. The saturation magnetisation and coercivity of Fe@SiO_2 nanocapsules prepared at 90°C with 900 µl TEOS are 43.05 emu g^{-1} and 708 Oe, while those of Fe@SiO_2 nanocapsules prepared at 120°C with 900 µl TEOS are 51.44 emu g^{-1} and 717 Oe, and Fe@SiO_2 nanocapsules prepared at 120°C with 100 µl TEOS are 123.48 emu g^{-1} and 674 Oe, respectively. It is obvious that the saturation magnetisation of Fe@SiO_2 nanocapsules decreases with increasing TEOS amount. This was due to the increase in shell thickness with increasing TEOS amount, as discussed in Fig. 4, which decreased the Fe fraction in each nanocapsule [33]. For Fe@SiO_2 nanocapsules prepared with 900 µl TEOS, the saturation magnetisation of nanocapsules prepared at 90°C is less than nanocapsules prepared at 120°C. This was due to the particles length of Fe@SiO_2 nanocapsules prepared at 90°C is shorter than nanocapsules prepared at 120°C, therefore, it has more surface area and coated more silica. Moreover, there has been little change among the coercivity of each Fe@SiO_2 nanocapsules. The coercivity of nanocapsules is independent of silica thickness and particles length, which is mainly influenced by the magnetic phase (iron particles). However, there are no significant changes in the size of Fe particles for each nanocapsule [5], as listed in Table 1. The coercivity of Fe@SiO_2 nanocomposites is higher than pristine Fe nanoparticles [8]. The magnetic moments of pristine Fe nanoparticles are oriented randomly, which led to the smaller value of magnetic anisotropy. In contrast, the silica-coated Fe nanoparticles lead to the ferromagnetic state and promote the higher magnetic anisotropy of the ensembles.

4. Conclusion: In summary, highly monodisperse Fe@SiO_2 core-shell nanocapsules with different particle size and different silica thickness were synthesised via hydrothermal reaction followed with heat treatment. The Fe@SiO_2 nanocapsules prepared at 90 and 120°C are relatively monodispersed with their mean size 328 and 546 nm, respectively. The silica thickness of Fe@SiO_2 nanocapsules prepared at 120°C with 100 and 900 µl TEOS are in the range of 10–20 and 25–35 nm, respectively. The saturation magnetisation of Fe@SiO_2 nanocapsules decreases with increasing silica thickness due to the volume fraction of Fe particles decreased. The particles length and silica thickness of Fe@SiO_2 nanocapsules have no significant influence on the coercivity of Fe@SiO_2 nanocapsules, owing to the size of Fe particles have little changed.

5. Acknowledgments: This work was supported by the National Key Technologies R&D Program (grant no. 2018YFC0115202), Scientific and Technological Research Program of Chongqing Municipal Education Commission (grant no. KJZD-M201801501), the Program for Innovation Teams in University of Chongqing (grant no. CXTDX201601032) and the Technology Innovation Project of Chongqing University of Science & Technology (grant no. YKJCX1820202).

6 References

[1] Jin H., Lilley C.M.: 'Surface effect on the elastic behavior of static bending nanowires', *Nano Lett.*, 2008, **8**, pp. 1798–1802
[2] Sichert J.A., Tong Y., Mutz N., *ET AL.*: 'Quantum size effect in organometal halide perovskite nanoplatelets', *Nano Lett.*, 2015, **15**, pp. 6521–6527
[3] Ramesh K.: 'Nanomaterials: mechanics and mechanisms' (Springer, Boston, 2009)
[4] Jing C., Xiaomin N.I., Zheng H., *ET AL.*: 'Preparation of Fe (core)/SiO_2 (shell) composite particles with improved oxidation-resistance', *Mater. Res. Bull.*, 2006, **41**, pp. 1424–1429
[5] Thirumal E., Prabhu D., Chattopadhyay K., *ET AL.*: 'Synthesis, magnetic and electrical properties of Fe-containing SiO_2 nanocomposite', *J. Alloys Compd.*, 2010, **502**, pp. 169–175
[6] Byoun W., Jang M., Yoo H.: 'Fabrication of highly fluorescent multiple Fe3O4 nanoparticles core-silica shell nanoparticles', *J. Nanopart. Res.*, 2019, **21**, pp. 1
[7] Yang T.I., Brown R.N.C., Kempel L.C., *ET AL.*: 'Controlled synthesis of core-shell iron-silica nanoparticles and their magneto-dielectric properties in polymer composites', *Nanotechnology*, 2011, **22**, p. 105601

doi: 10.1049/mnl.2019.0063

[8] Zelenakova A., Zelenak V., Mat'Ko I., *ET AL.*: 'Superferromagnetism in chain-like Fe@SiO_2 nanoparticle ensembles', *J. Appl. Phys.*, 2014, **116**, pp. 439–486
[9] Fu L., Jiang J., Xu C., *ET AL.*: 'Synthesis and electromagnetic properties of Fe/SiO_2 yolk/shell nanospheres with improved oxidation resistance', *Micro Nano Lett.*, 2013, **8**, pp. 349–352
[10] Li B., Qiao Y., An J., *ET AL.*: 'Synthesis, characterisation, and evaluation of core–shell Fe_3O_4/SiO_2/polypyrrole composite nanoparticles', *Micro Nano Lett.*, 2018, **13**, pp. 902–906
[11] Seo W.S., Jin H.L., Sun X., *ET AL.*: 'FeCo/graphitic-shell nanocrystals as advanced magnetic-resonance-imaging and near-infrared agents', *Nature Mater.*, 2006, **5**, pp. 971–976
[12] Wei X.W., Zhu G.X., Xia C.J., *ET AL.*: 'A solution phase fabrication of magnetic nanoparticles encapsulated in carbon', *Nanotechnology*, 2006, **17**, p. 4307
[13] Zhang N., Liu S., Fu X., *ET AL.*: 'Synthesis of M@TiO_2 (M = Au, Pd, Pt) core-shell nanoconnposites with tunable photoreactivity', *J. Phys. Chem. C*, 2011, **115**, pp. 9136–9145
[14] Xin T., Ma M., Zhang H., *ET AL.*: 'A facile approach for the synthesis of magnetic separable Fe_3O_4@TiO_2, core–shell nanocomposites as highly recyclable photocatalysts', *Appl. Surf. Sci.*, 2014, **288**, pp. 51–59
[15] Sun Z.C., Zussman E., Yarin A.L., *ET AL.*: 'Compound core–shell polymer nanofibers by Co-electrospinning', *Adv. Mater.*, 2010, **15**, pp. 1929–1932
[16] Ghosh Chaudhuri R., Paria S.: 'Core/shell nanoparticles: classes, properties, synthesis mechanisms, characterization, and applications', *Chem. Rev.*, 2012, **112**, pp. 2373–2433
[17] Longgang Y., Jianbo W., Xianghua H., *ET AL.*: 'Enhanced microwave absorption of Fe nanoflakes after coating with SiO_2 nanoshell', *Nanotechnology*, 2010, **21**, p. 095708
[18] Suying W., Qiang W., Jiahua Z., *ET AL.*: 'Multifunctional composite core-shell nanoparticles', *Nanoscale*, 2011, **3**, pp. 4474–4502
[19] Li Y. C., Jin Z. H., Li T.L.: 'A novel and simple method to synthesize SiO_2-coated Fe nanocomposites with enhanced Cr (VI) removal under various experimental conditions', *Desalination*, 2012, **288**, pp. 118–125
[20] Jeong U., Shin H.H., Kim Y.: 'Functionalized magnetic core–shell Fe@SiO_2 nanoparticles as recoverable colorimetric sensor for CO_2 + ion', *Chem. Eng. J.*, 2015, **281**, pp. 428–433
[21] Zhang C.W., Zeng C.C., Ying X.U.: 'Preparation and characterization of surface-functionalization of silica-coated magnetite nanoparticles for drug delivery', *Nano*, 2014, **9**, p. 1450042
[22] Qian L., Shang X., Zhang B., *ET AL.*: 'Enhanced removal of Cr(VI) by silicon rich biochar-supported nanoscale zero-valent iron', *Chemosphere*, 2019, **215**, pp. 739–745
[23] Chen Z., Wei D., Qian L., *ET AL.*: 'Macroscopic and microscopic investigation of Cr(VI) immobilization by nanoscaled zero-valent iron supported zeolite MCM-41 via batch, visual, XPS and EXAFS techniques', *J. Cleaner Prod.*, 2018, **181**, pp. 745–752
[24] Wei L., Ji M., Sun S., *ET AL.*: 'Gram-grade Cr (VI) adsorption on porous Fe@SiO_2 hierarchical microcapsules', *J. Water Process Eng.*, 2016, **12**, pp. 111–119
[25] Ensie B., Samad S.: 'Removal of nitrate from drinking water using nano SiO_2–FeOOH–Fe core–shell', *Desalination*, 2014, **347**, pp. 1–9
[26] Mofradnia S.R., Ashouri R., Tavakoli Z., *ET AL.*: 'Effect of zero-valent iron/starch nanoparticle on nitrate removal using MD simulation', *Int. J. Biol. Macromol.*, 2019, **121**, pp. 727–733
[27] Zhang Y.P., Douglas G.B., Kaksonen A.H., *ET AL.*: 'Microbial reduction of nitrate in the presence of zero-valent iron', *Sci. Total Environ.*, 2019, **646**, pp. 1195–1203
[28] Vollprecht D., Krois L.M., Sedlazeck K.P., *ET AL.*: 'Removal of critical metals from waste water by zero-valent iron', *J. Cleaner Prod.*, 2019, **208**, pp. 1409–1420
[29] Kishimoto N., Narazaki Y., Takemoto K.: 'Reusability of zero-valent iron particles for zinc ion separation', *Sep. Purif. Technol.*, 2018, **193**, pp. 139–146
[30] Wei C., Nan Z.: 'Effects of experimental conditions on one-dimensional single-crystal nanostructure of β-FeOOH', *Mater. Chem. Phys.*, 2011, **127**, pp. 220–226
[31] Yue J., Jiang X., Yu A.: 'Experimental and theoretical study on the β-FeOOH nanorods: growth and conversion', *J. Nanopart. Res.*, 2011, **13**, pp. 3961–3974
[32] Ozel F., Kockar H., Karaagac O.: 'Growth of iron oxide nanoparticles by hydrothermal process: effect of reaction parameters on the nanoparticle size', *J. Supercond. Novel Magn.*, 2015, **28**, pp. 823–829
[33] Xu H., Cui L., Tong N., *ET AL.*: 'Development of high magnetization Fe_3O_4/polystyrene/silica nanospheres via combined miniemulsion/emulsion polymerization', *J. Am. Chem. Soc.*, 2006, **128**, pp. 15582–15583